의학박사 학위논문

IDH 변이가 없는 (IDH-wildtype) 교모세포종의 영상 기반 시공간 종양 서식지에 대한 전향적 장기 분석: 다중인자 생리학적 자기공명 영상을 통한 환자 예후 예측

Prospective Longitudinal Analysis of Imaging-based Spatiotemporal Tumor Habitats in Glioblastoma, IDH-wildtype: Implication in Patient Outcome Using Multiparametric Physiologic MRI

울 산 대 학 교 대 학 원

의 학 과

문 혜 현

IDH 변이가 없는 (IDH-wildtype) 교모세포종의 영상 기반 시공간 종양 서식지에 대한 전향적 장기 분석: 다중인자 생리학적 자기공명 영상을 통한 환자 예후 예측

지 도 교 수　　박 지 은

이 논문을 의학박사 학위 논문으로 제출함

2024 년　2 월

울 산 대 학 교 대 학 원

의　　학　　과

문　혜　현

문혜현의 의학박사학위 논문을 인준함

심사위원	김호성	(인)
심사위원	정승채	(인)
심사위원	박지은	(인)
심사위원	구현정	(인)
심사위원	박예원	(인)

울 산 대 학 교 대 학 원

2024 년 2 월

Summary

Purpose: Physiologic MRI-based tumor habitat analysis has the potential to predict patient outcomes by identifying the spatiotemporal habitats of glioblastoma. This study aims to prospectively validate physiologic MRI-based tumor habitats for predicting time-to-progression (TTP) and the site of progression in isocitrate dehydrogenase (IDH)-wildtype glioblastoma patients following concurrent chemoradiotherapy (CCRT).

Materials and Methods: We prospectively enrolled 79 patients (mean age, 59.4 years ± 11.6 [SD]; 40 women; ClinicalTrials.gov ID: NCT02613988) with glioblastoma, IDH-wild who underwent CCRT. Immediate post-op and three serial MRI scans were obtained at three-month intervals, including diffusion-weighted imaging and dynamic susceptibility contrast imaging. Voxels from cerebral blood volume and apparent diffusion coefficient maps were grouped into 3 spatial habitats (hypervascular cellular, hypovascular cellular, and nonviable tissue) using k-means clustering. The pre-defined cutoff for the habitat risk score was applied (PMID: 33028594) with an increase in hypervascular cellular habitat (>0 voxel) or hypovascular cellular habitat (>130 voxels). Associations between spatiotemporal habitats, habitat risk score, and TTP were investigated using Cox proportional hazard modeling and Kaplan-Meier method. The site of progression was matched with the spatiotemporal habitats.

Results: An increase in hypervascular cellular habitat was associated with shorter TTP between post-op and post-CCRT #1 (Hazard ratio [HR], 72.41, P =.018). An increase in hypovascular cellular habitat was associated with shorter TTP between post-op and post-CCRT #1 (HR, 2.25, P =.010), post-CCRT #1-2 (HR, 51.60, P <.001), and post-CCRT #2-3 (HR, 3.52, P=.012). The habitat risk score between post-op and post-CCRT #1, post-CCRT #1-2, and post-CCRT #2-3 successfully stratified patients into low-, intermediate-, and high-

risk groups (log-rank test; P =.002, < .001, and .002, respectively). High habitat risk scores between post-op and post-CCRT#1 and post-CCRT #1-2 were independent predictors of TTP (P = .004 and P = .003, respectively) in multivariable Cox analysis. An increase in the hypovascular cellular habitat predicted tumor progression sites (mean DICE index: 0.31).

Conclusion: Spatiotemporal tumor habitats and habitat risk score derived from multiparametric physiologic MRI were validated as useful biomarkers for clinical outcomes in patients with IDH wild-type glioblastoma following CCRT. The hypovascular cellular habitat may serve as a robust imaging biomarker for predicting early tumor progression and identifying the site of progression.

Table of Contents

List of Tables

List of Figures

Introduction

Glioblastoma, renowned for its intratumoral heterogeneity, displays complex spatial variations in gene expression, histopathology, and macroscopic structure[1]. This heterogeneity contributes to a poor prognosis due to diverse treatment responses and the development of treatment resistance in different tumor regions[2]. Physiological MRI techniques, including cerebral blood volume (CBV) and apparent diffusion coefficient (ADC) mapping, enable the identification of distinct tumor regions with variations in metabolism, vascularity, and cellularity[3]. ADC provides insights into cell density and necrosis[4], while CBV is indicative of vessel density[5]. Some studies suggest improved accuracy in distinguishing between pseudoprogression and early tumor progression using quantitative parameters such as normalized CBV (nCBV) and ADC[4,6]. However, the challenge lies in the frequent coexistence of tumor recurrence and radiation injury in post-treatment glioblastoma[7], along with the tumor's inherent heterogeneity. Relying solely on individual quantitative parameters for evaluating post-treatment lesions is limiting, as a single parameter can offer only a probability in one direction or establish a linear correlation, restricting the comprehensive characterization of post-treatment glioblastoma[8]. While several imaging techniques, such as histograms, texture analysis, and radiomics, have been employed to quantify intratumoral heterogeneity based on imaging parameters, these methods often overlook spatial information, preventing the grouping of similar voxels[9,10].

To address this limitation, the concept of tumor habitat analysis has emerged as a promising strategy to delineate distinct subregions within a heterogeneous tumor by identifying voxels that share common tumor biology[11]. Through the application of voxel-wise clustering, this approach separates distinct tumor habitats via parcellation[12], offering valuable clinical insights into subregions associated with tumor progression, treatment resistance, and potential therapeutic targets[13]. Thus, clustering of multiparametric physiologic MRI, including diffusion-weighted and perfusion-weighted MRI, can reflect spatial habitats of post-treatment

glioblastoma following concurrent chemoradiation therapy (CCRT). Furthermore, analyzing the temporal changes in spatial habitats derived from multiparametric physiologic MRI could offer valuable insights into both spatial and temporal heterogeneity in post-treatment glioblastoma.

Our previous research[14] identified three distinct spatial habitats within post-treatment glioblastoma: hypervascular cellular, hypovascular cellular, and nonviable tissue habitats. Among these, an increase in the hypervascular cellular and hypovascular cellular habitat was associated with poor prognosis following CCRT. In addition, this study defined the habitat risk score based on the discrete increase of the hypervascular and hypovascular cellular habitats, demonstrating that these scores stratified patients into low-, intermediate-, and high-risk groups. Moreover, the localization of the hypovascular cellular correlated with the site of tumor progression. However, the actual clinical efficacy of physiological MRI-based spatiotemporal tumor habitats and habitat risk score in predicting early tumor progression and patient outcomes has not been validated in prospective studies.

In this study, we aim to prospectively validate physiologic MRI-based tumor habitat analysis in predicting TTP and identifying the site of progression after CCRT in patients with IDH-wild type glioblastoma.

Methods

This prospective single-center study was registered at ClinicalTrials.gov (ClinicalTrials.gov identifier: NCT02613988) and received approval from the Institutional Review Board (IRB) of Asan Medical Center (local approval number: 2019-1259). The study was conducted in compliance with the U.S. Health Insurance Portability and Accountability Act regulations and the Declaration of Helsinki. Written and signed informed consent was obtained from each participant prior to enrollment.

Study population

The inclusion process for the study patients was shown in **Figure 1**. Consecutive patients with a histopathologic diagnosis of IDH-wildtype glioblastoma, presenting a measurable contrast-enhancing lesion on MRI after CCRT at our institution between January 2020 and June 2022, and who had given written informed consent, were considered eligible. The patients were enrolled according to the follow inclusion criteria: (i) age ≥18 years; (ii) histopathologic diagnosis of IDH-wildtype glioblastoma according to the World Health Organization classification 2016[1] and 2021[15]; (iii) underwent current standard treatment: maximum safe surgical resection followed by CCRT and adjuvant temozolomide; (iv) had a measurable CEL of more than 1 x 1 cm^2 at the first post-CCRT examination; and (v) underwent conventional and advanced MRI, including diffusion-weighted imaging (DWI) and dynamic susceptibility contrast (DSC) imaging. The exclusion criteria were as follows: (i) insufficient follow-up with at least three successive imaging examinations or pathologic confirmation to monitor treatment response; and (ii) inadequate image quality.

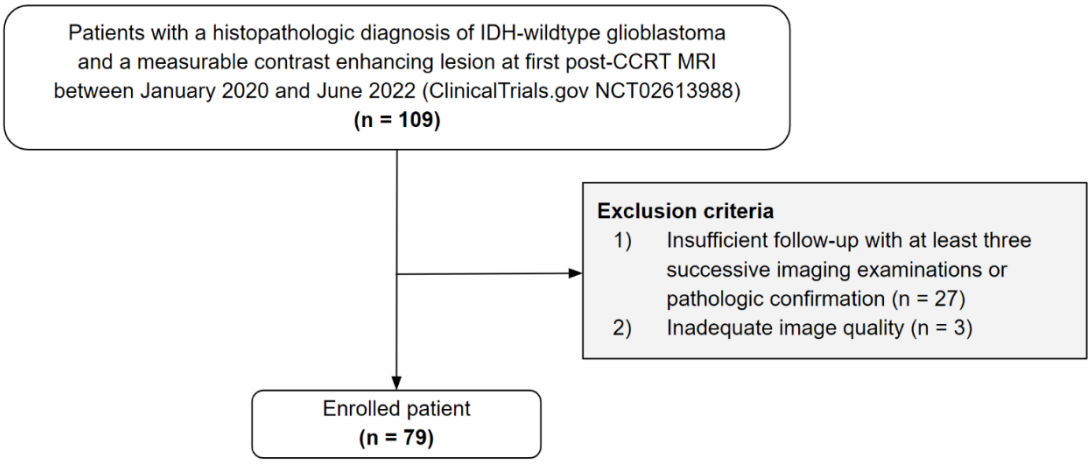

Figure 1. Flow diagram of the patient inclusion process. Abbreviation: CCRT = concurrent chemoradiotherapy; IDH = isocitrate dehydrogenase.

MRI acquisitions

The brain tumor imaging protocol was acquired on a 3-T scanner (Ingenia 3.0 CX, Philips Healthcare) and included both conventional and advanced sequences: T2-weighted imaging (T2WI), fluid-attenuated inversion recovery (FLAIR) imaging, T1-weighted imaging (T1WI), DWI, DSC perfusion imaging, and contrast-enhanced (CE) T1WI. The DWI parameters were as follows: repetition time (TR)/echo time (TE) at 3,000/56 ms, diffusion gradient encoding with b values of 0 and 1,000 seconds/mm^2, field of view (FOV) of 250 x 250 mm, matrix dimensions of 256 x 256, and a slice thickness/gap of 5/2 mm. ADC images were be calculated based on the DWI images acquired with b values of 1,000 and 0 second/mm^2. DSC imaging was conducted using a gradient-echo echo-planar imaging protocol. A preload of 0.01 mmol/kg gadoterate meglumine (Dotarem; Guerbet) was administered, followed by a dynamic bolus of a standard dose of 0.1 mmol/kg gadoterate meglumine at a rate of 4 mL/second using an MRI-compatible power injector (Spectris; Medrad). Subsequently, 20 mL of saline was injected at the same rate. The DSC imaging parameters were as follows: TR/TE of 1,808/40 ms, a flip angle of 35°, FOV of 24 x 24 cm, slice thickness/gap of 5/2 mm, matrix dimensions of 128 x 128, and a total acquisition time of 1 minute and 54 seconds. The dynamic acquisition will have a temporal resolution of 1.5 seconds, capturing a total of 60 dynamics. The DSC imaging covered the entire tumor volume with the same section orientation as conventional MRI.

Reference standard for final diagnosis and endpoints

Progression was pathologically confirmed through second-look operations if clinically indicated. In cases where second-look operations were not performed, consecutive clinicoradiological diagnoses were established by consensus between two experts: J.H. Kim, with 26 years of experience in neuro-oncology practice, and a neuroradiologist, H.S. Kim, with 21 years of experience in neuro-oncologic imaging. These diagnoses was based on the

RANO criteria[16] . Progression was defined as the occurrence of any new lesion outside the radiation field or a gradual increase in the size of the contrast-enhancing lesion observed in more than two subsequent follow-up MRI examinations conducted at 2–3-month intervals, necessitating a prompt change in treatment. The primary endpoint of the study is TTP, calculated from the day of initial diagnosis to the day of first documented progression. The secondary endpoint is the site of progression.

Mask segmentation and advanced image processing

To process the three-dimensional contrast-enhanced T1-weighted imaging (3D CE T1WI) and FLAIR data, a skull stripping algorithm optimized for heterogeneous MRI data was employed (https://github.com/MIC-DKFZ/HD-BET). Lesion segmentation masks were generated using a 3D UNet-based method (https://github.com/MIC-DKFZ/nnUNet; ref. 20) from the PyTorch package version 1.1 in Python 3.7 (www.python.org).

For the DSC analysis, pharmacokinetic map calculation was performed using Nordic ICE (NordicNeuroLab). The integrated DSC module incorporates a relative CBV (rCBV) leakage correction algorithm and manual noise thresholding to quantify the amount of blood in a given volume of tissue, expressed as mL per 100 mL tissue. The Weisskoff-Boxerman method, which calculates pixel-wise concentration-time curve deviations from a reference curve, was used for calculations assumed to be unaffected by leakage[17]. The rCBV maps were normalized based on the normal-appearing white matter to create normalized CBV (nCBV) maps.

To analyze changes across consecutive scans, the 3D CE T1WI images obtained from each patient were coregistered and resampled to have isometric-voxel sizes. Subsequently, FLAIR, nCBV, and ADC images were coregistered and resampled to the iso-voxel CE T1WI images using rigid transformations with six degrees of freedom in the SPM package (version 12, www.fil.ion.ucl.ac.uk/spm/). This step ensures continuous slices without gaps and

facilitates voxel-wise analysis for tracking habitats. The final voxel classifications based on nCBV and ADC values were implemented using a k-means clustering module in the scikit-learn python package.

Multiparametric physiologic MRI-based spatiotemporal habitat analysis

Population-level clustering based on previous research

Using two distinct feature maps, three clusters were established: cluster 1 represented the "hypervascular cellular tumor" with high CBV value and low ADC value, cluster 2 represented the "hypovascular cellular tumor" with low CBV value and low ADC value, and cluster 3 represented the "nonviable tissue" with low CBV value and high ADC value. The range for the boundary of the pre-trained and retrospectively validated spatial physiologic habitats was previously reported as 4.37–4.44 for nCBV and 150–187 (×10-6 mm^2/s) for ADC[14].

Calculation of spatiotemporal habitats and habitat risk score

Four consecutive MR examinations were used in the analysis: immediate post-operation (examination 1, post-op), the first visit after CCRT (examination 2, post-CCRT #1), the second visit after CCRT (examination 3, post-CCRT #2), and the third visit after CCRT (examination 4, post-CCRT #3), with a 3-month interval between each examination. Firstly, changes in the number of voxels within the entire contrast enhancing lesion and within each habitat were calculated between sequential examinations. Secondly, the habitat risk score, determined by the discrete increase in hypervascular and hypovascular cellular habitats between sequential examinations, was calculated. The cutoff for the discrete score was defined as an increase of more than 0 voxels for hypervascular cellular habitat or an increase of more than 130 voxels for hypovascular cellular habitat, as established in the previous study[14]. For example, when a patient showed an increase of both hypervascular cellular habitat (> 0 voxel) and hypovascular cellular habitat (>130 voxel), the habitat risk score was 2.

Analysis of site of progression

The site of progression was analyzed based on the follow-up examination at the time of progression. The volume of CEL at the time of progression was matched with the habitats identified in examination 2 (post-CCRT#1) or 3 (post-CCRT #2). The overlap between each spatiotemporal habitat and the CEL volume at the time of progression was quantified using the DICE similarity coefficient, $DICE = 2|P \cap R|/(|P|+|R|)$[18]. P represents each spatiotemporal habitat and R represents the CEL volume at the time of progression. The DICE ranges between 0 (no overlap) and 1 (perfect agreement). When tumor progression was diagnosed by surgical excision without follow-up MRI examination, the site of tumor progression could not be determined.

The overall process of tumor habitat analysis is shown in **Figure 2**.

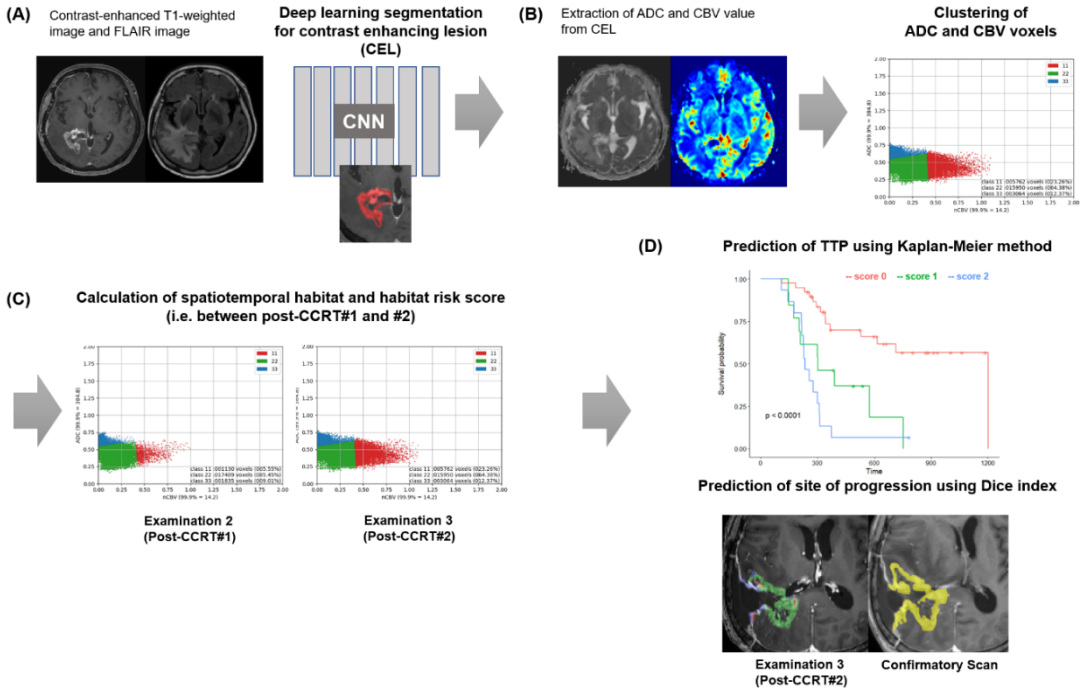

Figure 2. The overall process of tumor habitat analysis. (A) Image acquisition, registration, and deep learning segmentation of the contrast enhancing lesion (CEL). (B) Extraction of ADC and CBV value from CEL and voxel classifications based on ADC and CBV values. Three clusters were established using k-means clustering: hypervascular cellular habitat, hypovascular cellular habitat, nonviable tissue habitat. (C) Calculation of spatiotemporal habitats and habitat risk score between sequential examinations. (D) Associations of spatiotemporal habitats and time to progression and the site of progression were analyzed. Abbreviation: ADC = apparent diffusion coefficient; CBV= cerebral blood volume; CCRT = concurrent chemoradiotherapy; TTP = time to progression

Statistical analysis

Baseline characteristics including sex, age, Karnofsky performance score (KPS; binary, score >70 or ≤70), initial tumor volume, O6-methylguanine-DNA-methyltransferase (MGMT) promoter status, and extent of surgery were analyzed using descriptive statistics.

Power calculation - The methodology written here adheres to the REMARK (Reporting Recommendations for Tumor Marker Prognostic Studies) recommendations [19]. The sample size was calculated according to the Cox proportional hazards regression model with nonbinary covariates[20]. Death rates of 0.5~1.0 represent 51 deaths, with a sample size between 51 to 102 patients yielding expected power of 80% and an alpha error of 5%.

Use of spatiotemporal habitat to predict TTP - To analyze the association between spatiotemporal habitats and TTP, univariable analysis was conducted using Cox proportional hazard regression. Hazard ratios indicate relative change in hazard incurred by 1 unit increase in each parameter; 20000 voxels (20k voxels) defined a single unit in a previous study [14].

Risk stratification using habitat risk score - To analyze the association between habitat risk score and TTP, univariable and multivariable analysis was conducted using Cox proportional hazard regression. Risk stratification into high-, intermediate-, and low-risk categories, based on the habitat risk score, was analyzed using the Kaplan-Meier method (log-rank test).

All statistical analyses were conducted using the R Statistical Package (version 3.6.3, Institute for Statistics and Mathematics, http://www.R-project.org). A p-value less than 0.05 was considered statistically significant.

Results

Patient characteristics

Of the 109 potentially eligible patients, 27 with insufficient follow-up and 3 with inadequate image quality were excluded. Finally, 79 patients, 39 (49.4%) men and 40 (49.6%) women, with a mean age of 59.4 years ± 11.6 (SD) (range, 28–78 years), were included in the analysis. The baseline clinical characteristics of the 79 patients are summarized in **Table 1**. Among a total of 79 patients, 53 (67.1%) underwent maximal contrast-enhancing (CE) resection, 16 (20.3%) underwent submaximal CE resection, and 10 (12.7%) underwent a biopsy. Final diagnosis was based on pathologic confirmation for 18 (22.8%) patients and clinicoradiologic follow-up for 61 (77.2%) patients.

Table 1. Baseline clinical characteristics of the study patients

Clinical characteristics (n = 79)	
Sex, n, Male/female	39 / 40
Age, years, mean ± SD	59.4 ± 11.6
KPS at base line, n (%)	
> 70	64 (81.0%)
≤ 70	15 (19.0%)
MGMT promotor status, n (%)	
Methylated	33 (41.8%)
Unmethylated	35 (44.3%)
NA	11 (13.9%)
RANO* categories for the extent of resection, n (%)	
Supramaximal CE resection	0 (0%)
Maximal CE resection	53 (67.1%)
Submaximal CE resection	16 (20.3%)
Biopsy	10 (12.7%)
Secondary treatment after recurrence	
Surgery	18 (22.8%)
Bevacizumab	30 (38.0%)
Temozolomide	2 (2.5%)
Others	3 (3.8%)
NA	26 (32.9%)

Abbreviations: KPS = Karnofsky performance score; MGMT = O6-methylguanine DNAmethyltransferase gene methylation status; NA = information not available

*Referrers to the RANO resect group, an international multicenter group from seven neuro-oncological centers in US and Europe.

Spatiotemporal habitats associated with TTP

The results of the univariable analysis to evaluate the association between changes in three spatiotemporal habitats and TTP are summarized in **Table 2**. Between post-op and post-CCRT #1 examinations, both an increase in the hypervascular cellular habitat and an increase in hypovascular cellular habitat were significantly associated with short TTP (HR, 72.41; 95% CI, 2.10–2469.70; $P = .018$ and HR, 2.25; 95% CI, 1.21–4.18; $P = .010$, respectively). Between post-CCRT #1 and #2 examinations, an increase in hypovascular cellular habitat was significantly associated with a short TTP (HR, 51.60; 95% CI, 7.36–361.89; $P < .001$). Between post-CCRT #2 and #3 examinations, an increase in hypovascular cellular habitat was significantly associated with a short TTP (HR, 3.52; 95% CI, 1.31–9.42; $P = .012$). Among various changes in spatial habitats, an increase in the hypovascular cellular habitat (20 k voxels) was consistently associated with a relatively short TTP. **Figure 3** and **Figure 4** demonstrates the association between changes in three spatial habitat and TTP. An increase in both hypervascular cellular habitat and hypovascular cellular habitat was associated with short TTP, while an increase in nonviable tissue was not associated with TTP.

Table 2. Univariable analysis of the spatial habitat to predict time to progression in post-treatment IDH-wildtype glioblastoma patients.

	Time to progression		
	Hazard ratio	**95% CI**	***P***
Changes between post-op and post-CCRT #1			
Increase in hypervascular cellular habitat	72.41	2.10-2469.7	**.018**
Increase in hypovascular cellular habitat	2.25	1.21-4.18	**.010**
Increase in nonviable tissue habitat	2.04	0.57-7.31	.273
Changes between post-CCRT #1 and #2			
Increase in hypervascular cellular habitat	34.30	0.00-7277389	.572
Increase in hypovascular cellular habitat	51.60	7.36-361.89	**<.001**
Increase in nonviable tissue habitat	2.11	0.51-8.74	.304
Changes between post-CCRT #2 and #3			
Increase in hypervascular cellular habitat	8.46	0.07-1027.76	.383
Increase in hypovascular cellular habitat	3.52	1.31-9.42	**.012**
Increase in nonviable tissue habitat	1.32	0.01-284.52	.920

Note: Hazard ratios reported here indicate the relative change in hazard that a 1-unit (20,000 voxels) increase in each imaging parameter incurs. Abbreviation: IDH = isocitrate dehydrogenase; CCRT = concurrent chemoradiotherapy

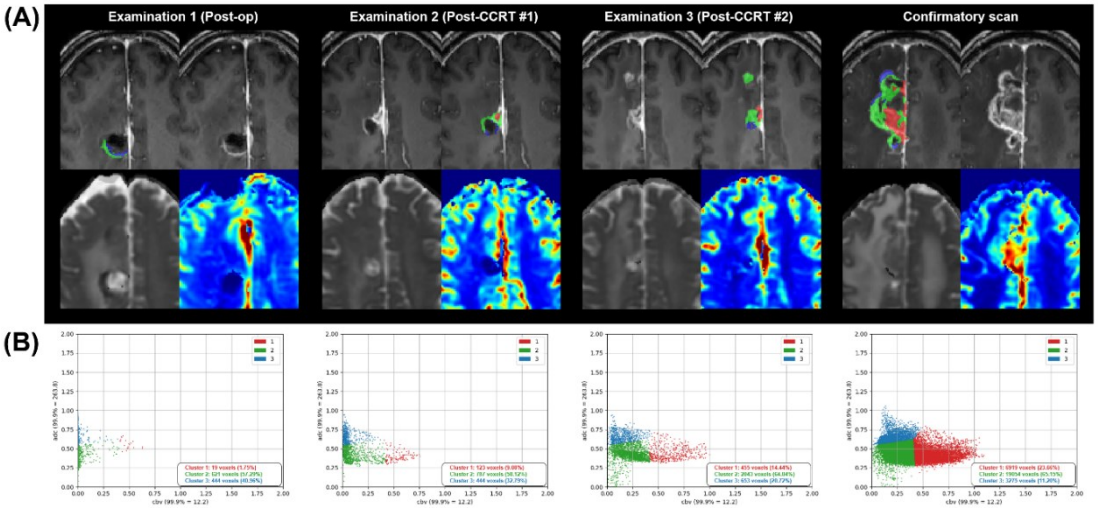

Figure 3. Representative case of tumor habitat analysis from a 64-year-old patient. The hypervascular cellular habitat (red color) shows high nCBV and low ADC, the hypovascular cellular habitat (green color) shows low nCBV and low ADC, and the nonviable tissue habitat (blue color) shows low nCBV and high ADC. **(A)** Spatial mapping shows an increase in both hypervascular and hypovascular cellular habitat in post-CCRT examinations. The confirmatory scan after 4 weeks indicates tumor progression. **(B)** Spatial habitats defined by clustered voxels. Between postop and post-CCRT #1 examinations, the hypervascular cellular habitat increased by 104 voxels, and the hypovascular cellular habitat by 166 voxels, resulting in a habitat risk score of 2 points. Between post-CCRT first and second scans, hypervascular cellular habitat increased by 332 voxels, hypovascular cellular habitat by 1256 voxels, resulting in a habitat risk score of 2 points. Abbreviation: nCBV= normalized cerebral blood volume; ADC = apparent diffusion coefficient; CCRT = concurrent chemoradiotherapy

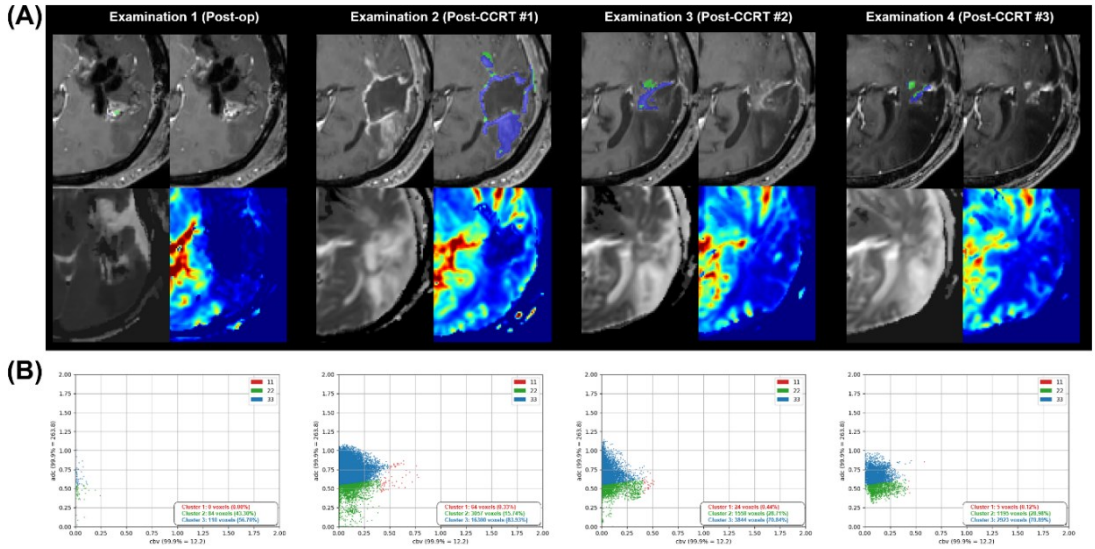

Figure 4. Representative case of tumor habitat analysis from a 37-year-old patient. (**A**) Spatial mapping in the post-CCRT #1 examination shows a newly developed measurable contrast enhancing lesion, but the majority of the lesion is considered nonviable tissue, showing low nCBV and high ADC values. Subsequent follow-up examinations demonstrate a gradual regression of the enhancing lesion, indicating pseudoprogression. (**B**) Spatial habitats defined by clustered voxels demonstrate a predominant increase in nonviable between post-op and post-CCRT #1 examinations. Abbreviation: CCRT = concurrent chemoradiotherapy; nCBV= normalized cerebral blood volume; ADC = apparent diffusion coefficient

Risk stratification based on the habitat risk score

The results of the univariable analysis to evaluate association between habitat risk score and TTP are summarized in **Table 3**. Between post-op and post-CCRT #1 examinations, habitat risk score of 2 was significantly associated with a short TTP (HR, 4.01; 95% CI, 1.76–9.13; $P = .001$). Between post-CCRT #1 and #2 examinations, both habitat risk score 1 and 2 were significantly associated with short TTP (HR, 3.38; 95% CI, 1.47–7.77; $P = .004$ and HR, 6.07; 95% CI, 2.78–13.24; $P < .001$, respectively). Between post-CCRT #2 and #3 examinations, habitat risk score of 2 was significantly associated with a short TTP (HR, 5.24; 95% CI, 1.92–14.35; $P = .001$). A high habitat risk score was consistently associated with a relatively short TTP.

The habitat risk score between post-op and post-CCRT #1, post-CCRT #1 and #2, and post-CCRT #2 and 3 examinations stratified patients into low-, intermediate-, and high-risk groups (log-rank test; $P = .002$, $< .001$, and .002, respectively, **Figure 5**).

A multivariable Cox analysis was conducted with the habitat risk score, age, KPS scores, extent of surgery, and MGMT methylation status as factors. Only the habitat risk score was identified as an independent predictor of TTP. Habitat risk score of 2 between post-op and post-CCRT #1 and post-CCRT #1 and #2 examinations was significantly associated with a relatively short TTP (HR, 4.44; 95% CI 1.59-12.42; $P = .004$ and HR, 6.13; 95% CI 1.83-20.48; $P = .003$ respectively).

Table 3. Univariable analysis of the habitat risk score to predict time to progression in post-treatment IDH-wildtype glioblastoma patients.

	Time to progression		
	Hazard ratio	**95% CI**	***P***
Between post-op and post-CCRT #1			
Habitat risk score 0	Ref		
Habitat risk score 1	2.33	0.95-5.70	.064
Habitat risk score 2	4.01	1.76-9.13	**.001**
Between post-CCRT #1 and #2			
Habitat risk score 0	Ref		
Habitat risk score 1	3.38	1.47-7.77	**.004**
Habitat risk score 2	6.07	2.78-13.24	**<.001**
Between post-CCRT #2 and #3			
Habitat risk score 0	Ref		
Habitat risk score 1	2.78	0.96-8.05	.059
Habitat risk score 2	5.24	1.92-14.35	**.001**

Abbreviation: IDH = isocitrate dehydrogenase; CCRT = concurrent chemoradiotherapy

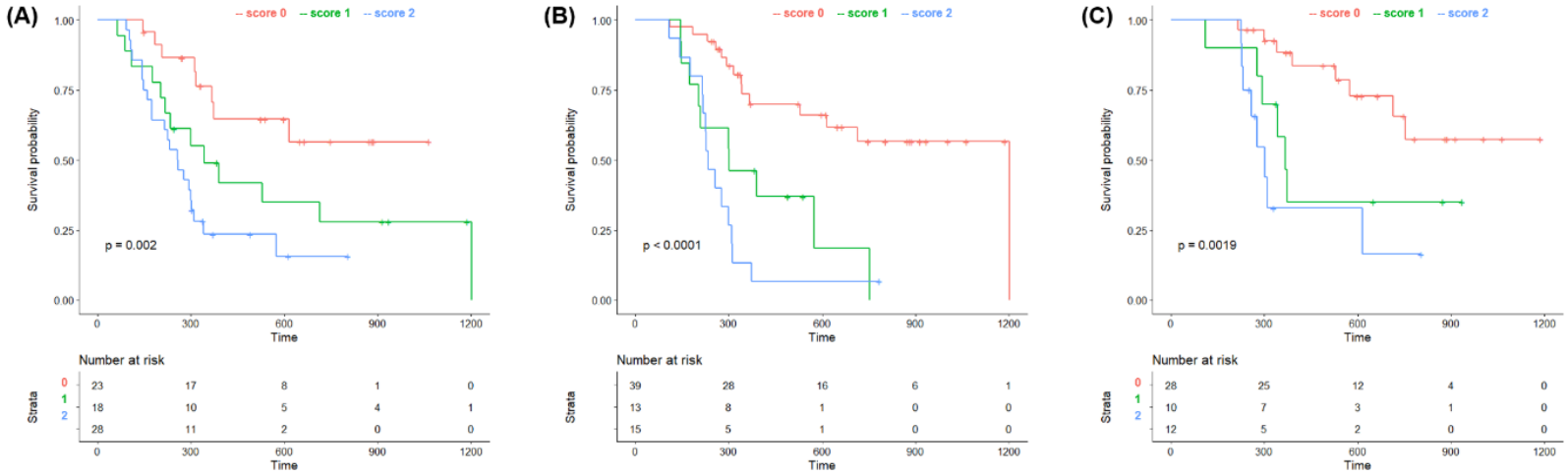

Figure 5. Kaplan–Meier survival curves for post-treatment IDH-wildtype glioblastoma patients according to habitat risk scores between (**A**) post-op and post-CCRT #1 examinations; (**B**) post-CCRT #1 and #2 examinations; and (**C**) post-CCRT #2 and #3 examinations. The habitat risk score successfully stratified patients into low-, intermediate-, and high-risk groups. Cross-hatches represent censored data. Abbreviation: IDH = isocitrate dehydrogenase; CCRT = concurrent chemoradiotherapy

Spatiotemporal habitats and site of progression

Out of the 49 patients who demonstrated progression, 25 (51%) had the DICE index calculated for the site of progression. The mean DICE index was 0.02 (range, 0–0.15; SD 0.03) for hypervascular cellular habitat, 0.31 (range, 0.06–0.66; SD 0.16) for hypovascular cellular habitat, and 0.20 for nonviable tissue (range, 0–0.64; SD, 0.15). The DICE index for the hypovascular cellular habitat was highest in 17 of the 25 cases (68%). **Figure 6** demonstrates representative cases illustrating the relationship between temporal changes in the hypovascular cellular habitat and the site of progression.

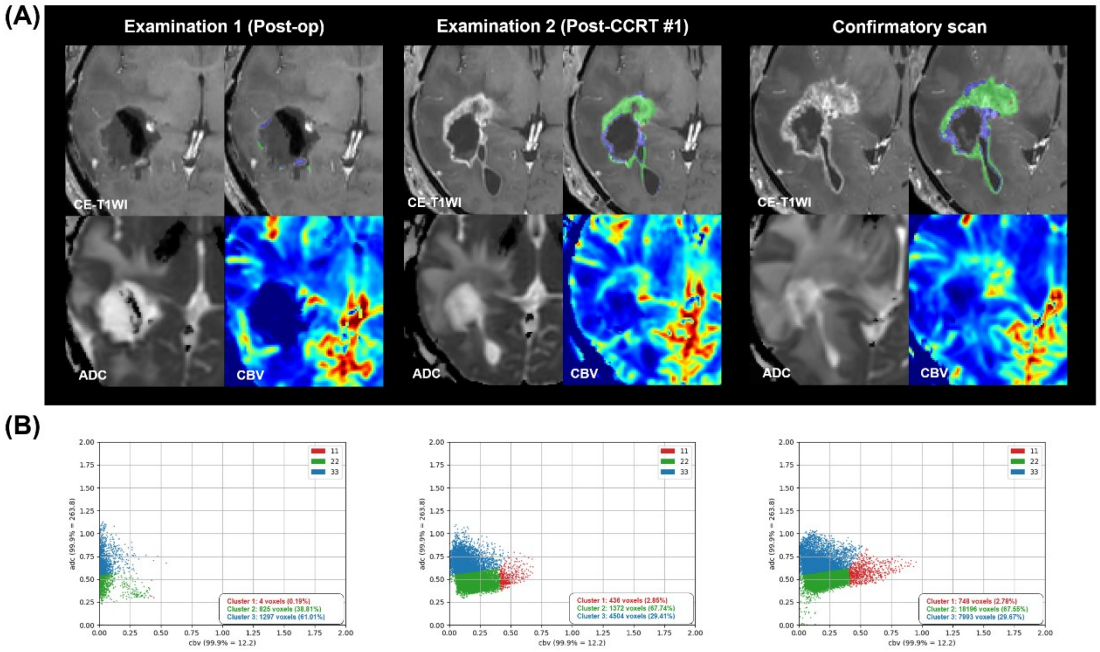

Figure 6. Representative case showing the relationship between the increase in the hypovascular cellular habitat and site of progression in a 59-year-old patient. (**A**) Spatial mapping shows an increase in the hypovascular cellular habitat at the anterior portion of the surgical cavity at post-CCRT#1 examination, 4 weeks after the completion of CCRT. Subsequently, the hypovascular cellular habitat became the site of progression at the 2-month follow-up with a confirmatory scan. (**B**) Three spatial habitats in this patient are defined by clustered voxels. Abbreviation: CCRT = concurrent chemoradiotherapy

Discussion

In this study, we prospectively validated multiparametric physiologic MRI-based tumor habitat analysis in predicting TTP and the site of progression in IDH wild-type glioblastoma patients after CCRT. An increase in the hypovascular cellular habitat with both low ADC and CBV values showed the most significant association with TTP and predicted the site of progression. The habitat risk score successfully stratified patients into low-, intermediate-, and high-risk group for early tumor progression.

Apart from changes induced by treatment, such as decreased perfusion and increased diffusion, the post-treatment glioblastoma tissues could demonstrate a spectrum of perfusion levels from low to high, along with decreased diffusion[21]. Spatiotemporal habitats, defined by both ADC and CBV values, enable the prediction of patient outcomes by quantifying the initial pathophysiologic changes in post-treatment glioblastoma. Analyzing spatiotemporal habitats is more effective than relying on a singular snapshot when predicting TTP in post-treatment glioblastomas, given the inherent variability in the histopathology of these tumors [22]. Although the hypervascular cellular habitat, characterized by high CBV and low ADC values, represents the most malignant region of a tumor, an increase in the hypovascular cellular habitat with both low ADC and CBV values showed the most significant association with TTP at all-time points. This result aligns with our previous retrospective study conducted with a sample of 97 IDH-wildtype glioblastoma patients[14]. The hypovascular cellular habitat identified in our study may indicate a hypoxic microenvironment resistant to treatment, featuring changes in gene and molecular expression and evolution toward increased malignancy and a more aggressive phenotype [23]. Moreover, low CBV values may represent a decrease in the patent vessels delivering the chemotherapeutic agent to the tumor bed, consequently inducing resistance to treatment.

The habitat risk score, based on the discrete increase of hypervascular and

hypovascular cellular habitats, successfully stratified patients' risk and was identified as an independent predictor of TTP. We employed the previously defined cut-off from our retrospective study[14] to calculate the habitat risk score and prospectively validated both cut-off of the habitat risk score and its predictive value for patient outcomes. Utilizing the habitat risk score, changes in spatiotemporal habitats can be easily determined, potentially aiding in the stratification of patients with glioblastoma based on the risk of early progression. While this study was conducted at the same single center, we believe that a prospective multicenter study is necessary for further validation.

The spatiotemporal habitat is valuable not only for predicting patient outcomes but also for identifying tumor subregions associated with tumor progression and treatment resistance. Through quantitative analysis of the DICE index, we observed a correlation between tumor progression foci and regions exhibiting a short-term increase in the hypovascular cellular habitat, with the latter demonstrating the highest DICE index alignment with CEL at the time of progression. In the context of recurrent glioblastoma, re-resection is limited [24], and the presence of spatial heterogeneity in post-treatment glioblastoma poses challenges in obtaining adequate lesion samples for effective histological analysis. Even with sufficient tissue sampling, there are currently no explicit standards for histologic diagnosis of pseudoprogression, residual glioma, and recurrent glioma[25]. In this study, we have demonstrated the capability of multiparametric physiologic MRI-based tumor habitat analysis to non-invasively pinpoint the site of progression. Furthermore, employing radiographic guidance through this method is expected to enhance the effectiveness of obtaining optimal tissue samples in cases of recurrent glioblastoma.

This study has several limitations. Firstly, there was a lack of strict pathological correlations with image-based segmentation. We were thus unable to determine whether these three spatial habitats were pathologically identical or not. However, establishing such

correlations would be highly challenging, and it is crucial to avoid unnecessary surgery. Secondly, the three habitats described in this study are relative indices of cellular environments, displaying ADC values that are relatively lower compared to those of other habitats. The b-values chosen in our study were restricted to b = 0 and b = 1,000 seconds/mm^2, introducing a potential risk of perfusion contamination in ADC values. Thirdly, this study was conducted at a single center. Therefore, it is essential to apply different protocols from other institutions with a relatively large number of patients for broader validation. Lastly, our study included 10 patients (12.7%) who underwent biopsy only, and a future subgroup analysis based on the extent of resection was deemed necessary.

Conclusions

In conclusion, multiparametric physiologic MRI-based spatiotemporal tumor habitats derived from immediate post-CCRT imaging were validated as a useful biomarker for early tumor progression and clinical outcomes in patients with IDH-wildtype glioblastoma. An increase in the hypovascular cellular habitat can be considered a robust imaging biomarker for predicting early tumor progression and identifying the site of progression.

References

1. Louis DN, Perry A, Reifenberger G, et al. The 2016 World Health Organization classification of tumors of the central nervous system: a summary. *Acta neuropathologica* 2016; **131**: 803-20.
2. Shipitsin M, Campbell LL, Argani P, et al. Molecular definition of breast tumor heterogeneity. *Cancer cell* 2007; **11**(3): 259-73.
3. John F, Bosnyák E, Robinette NL, et al. Multimodal imaging-defined subregions in newly diagnosed glioblastoma: impact on overall survival. *Neuro-oncology* 2019; **21**(2): 264-73.
4. Asao C, Korogi Y, Kitajima M, et al. Diffusion-weighted imaging of radiation-induced brain injury for differentiation from tumor recurrence. *American Journal of Neuroradiology* 2005; **26**(6): 1455-60.
5. Fatterpekar GM, Galheigo D, Narayana A, Johnson G, Knopp E. Treatment-related change versus tumor recurrence in high-grade gliomas: a diagnostic conundrum—use of dynamic susceptibility contrast-enhanced (DSC) perfusion MRI. *American Journal of Roentgenology* 2012; **198**(1): 19-26.
6. Sugahara T, Korogi Y, Tomiguchi S, et al. Posttherapeutic intraaxial brain tumor: the value of perfusion-sensitive contrast-enhanced MR imaging for differentiating tumor recurrence from nonneoplastic contrast-enhancing tissue. *American Journal of Neuroradiology* 2000; **21**(5): 901-9.
7. Jung V, Romeike BF, Henn W, et al. Evidence of focal genetic microheterogeneity in glioblastoma multiforme by area-specific CGH on microdissected tumor cells. *Journal of neuropathology and experimental neurology* 1999; **58**(9): 993-9.
8. Park JE, Kim HS, Goh MJ, Kim SJ, Kim JH. Pseudoprogression in patients with glioblastoma: assessment by using volume-weighted voxel-based multiparametric clustering of MR imaging data in an independent test set. *Radiology* 2015; **275**(3): 792-802.
9. Alic L, Niessen WJ, Veenland JF. Quantification of heterogeneity as a biomarker in tumor imaging: a systematic review. *PloS one* 2014; **9**(10): e110300.
10. Just N. Improving tumour heterogeneity MRI assessment with histograms. *British journal of cancer* 2014; **111**(12): 2205-13.
11. O'Connor JP, Rose CJ, Waterton JC, Carano RA, Parker GJ, Jackson A. Imaging Intratumor Heterogeneity: Role in Therapy Response, Resistance, and Clinical OutcomeImaging Intratumor Heterogeneity. *Clinical Cancer Research* 2015; **21**(2): 249-57.
12. O'Connor JP, Rose CJ, Waterton JC, Carano RA, Parker GJ, Jackson A. Imaging intratumor heterogeneity: role in therapy response, resistance, and clinical outcome. *Clinical Cancer Research* 2015; **21**(2): 249-57.
13. Dextraze K, Saha A, Kim D, et al. Spatial habitats from multiparametric MR imaging are associated with signaling pathway activities and survival in glioblastoma. *Oncotarget* 2017; **8**(68): 112992.
14. Park JE, Kim HS, Kim N, Park SY, Kim Y-H, Kim JH. Spatiotemporal Heterogeneity in Multiparametric Physiologic MRI Is Associated with Patient Outcomes in IDH-Wildtype GlioblastomaMRI-Based Spatiotemporal Habitats for Glioblastoma. *Clinical Cancer Research* 2021; **27**(1): 237-45.
15. Louis DN, Perry A, Wesseling P, et al. The 2021 WHO classification of tumors of the central nervous system: a summary. *Neuro-oncology* 2021; **23**(8): 1231-51.
16. Wen PY, Macdonald DR, Reardon DA, et al. Updated response assessment criteria for high-grade gliomas: response assessment in neuro-oncology working group. *Journal of clinical oncology* 2010; **28**(11): 1963-72.
17. Weisskoff R, Boxerman J, Sorensen A, Kulke S, Campbell T, Rosen B. Simultaneous blood volume and permeability mapping using a single Gd-based contrast injection.

Proceedings of the Society of Magnetic Resonance, second annual meeting; 1994; 1994. p. 6-12.
18. Dice LR. Measures of the amount of ecologic association between species. *Ecology* 1945; **26**(3): 297-302.
19. Altman DG, McShane LM, Sauerbrei W, Taube SE. Reporting recommendations for tumor marker prognostic studies (REMARK): explanation and elaboration. *BMC medicine* 2012; **10**(1): 1-39.
20. Hsieh F, Lavori PW. Sample-size calculations for the Cox proportional hazards regression model with nonbinary covariates. *Controlled clinical trials* 2000; **21**(6): 552-60.
21. Prager A, Martinez N, Beal K, Omuro A, Zhang Z, Young R. Diffusion and perfusion MRI to differentiate treatment-related changes including pseudoprogression from recurrent tumors in high-grade gliomas with histopathologic evidence. *American Journal of Neuroradiology* 2015; **36**(5): 877-85.
22. Melguizo-Gavilanes I, Bruner JM, Guha-Thakurta N, Hess KR, Puduvalli VK. Characterization of pseudoprogression in patients with glioblastoma: is histology the gold standard? *Journal of neuro-oncology* 2015; **123**: 141-50.
23. Knisely JP, Rockwell S. Importance of hypoxia in the biology and treatment of brain tumors. *Neuroimaging Clinics* 2002; **12**(4): 525-36.
24. Dardis C, Ashby L, Shapiro W, Sanai N. Biopsy vs. extensive resection for first recurrence of glioblastoma: is a prospective clinical trial warranted? *BMC Research Notes* 2015; **8**: 1-9.
25. Haider AS, Van Den Bent M, Wen PY, et al. Toward a standard pathological and molecular characterization of recurrent glioma in adults: a response assessment in neuro-oncology effort. *Neuro-oncology* 2020; **22**(4): 450-6.

국문요약

IDH 변이가 없는 (IDH-wildtype) 교모세포종의 영상 기반 시공간 종양 서식지에 대한 전향적 장기 분석: 다중인자 생리학적 자기공명 영상을 통한 환자 예후 예측

문 혜 현

울산대학교 대학원 의학과

서론: 생리학적 자기 공명 영상(MRI)을 기반으로 한 종양 서식지 분석은 교모세포종의 시공간 서식지를 식별함으로써 환자 결과를 예측할 수 있는 잠재력이 있다. 본 연구는 IDH 변이가 없는 IDH-wildtype) 교모세포종 환자들에서 동시 화학 방사선 치료 (concurrent chemoradiotherapy, CCRT) 후 진행 시간 (time to progression, TTP) 및 진행 위치를 예측하기 위해 생리학적 MRI 기반 종양 서식지를 전향적으로 검증하는 것을 목적으로 하였다.

방법: 본 연구에서는 CCRT 를 받은 79 명의 IDH-wildtype 교모세포종 환자들을 전향적으로 등록하였다 (평균 연령 59.4 세 ± 11.6 [표준편차]; 여성 40 명; ClinicalTrials.gov ID: NCT02613988). 수술 직후 및 3 개월 간격으로 3 회의 일련의 MRI 검사 수행되었으며, 확산 가중 영상 (diffusion-weighted imaging) 및 동적 감수성 대조 영상 (dynamic susceptibility contrast imaging)이 포함되었다. 뇌 혈류량 (cerebral blood volume) 및 표면 확산 계수 지도 (apparent diffusion coefficient maps)에서의 voxel 은 k-means clustering 을 사용하여 3 개의 공간 서식지 (과잉 혈관 세포, 저혈관 세포, 비활성 조직)로 그룹화 되었다. 서식지 위험 점수 (habitat risk score)에 대해서는 미리 정의된 기준 (PMID: 33028594)으로, 과잉 혈관 세포 서식지 (>0 voxel) 또는 저혈관 세포 서식지 (>130 voxel) 증가가 적용되었다. 시공간 서식지, 서식지 위험 점수 및 TTP 간의 관련성은 Cox 비례

위험 모델 및 Kaplan-Meier 방법을 사용하여 분석되었다. 진행 위치는 시공간 서식지와 비교되었다.

결과: 수술 후와 CCRT 첫번째 검사 사이에서의 과잉 혈관 세포 서식지 증가는 의 짧은 TTP 와 연관이 있었다 (위험 비율 [Hazard ratio, HR], 72.41, *P* =.018). 수술 후와 CCRT 첫 번째 검사, CCRT 첫 번째와 두 번째 검사, 그리고 CCRT 두 번째와 세 번째 검사 사이에서의 저혈관 세포 서식지의 증가는 의 짧은 TTP 와 연관이 있었다 (HR, 2.25, *P* =.010; HR, 51.60, *P* <.001; HR, 3.52, *P*=.012) . 수술 후와 CCRT 첫 번째 검사, CCRT 첫 번째와 두 번째 검사, CCRT 두 번째와 세 번째 검사 간의 서식지 위험 점수는 환자를 저위험, 중위험 및 고위험 그룹으로 성공적으로 계층화 하였다 (log-rank test; *P* =.002, < .001, .002). 수술 후와 CCRT 첫 번째 검사, CCRT 첫 번째와 두 번째 검사 간의 높은 서식지 위험 점수는 다변량 Cox 분석에서 TTP 의 독립적인 예측 변수였다 (*P*=.004 및 *P*=.003). 저혈관 세포 서식지의 증가는 종양 진행 위치를 예측했다 (평균 DICE 지수: 0.31).

결론: 본 연구를 통해 다중 매개 변수 생리학적 MRI 로 유도된 시공간 종양 서식지 및 서식지 위험 점수는 CCRT 후 IDH-wildtype 교모세포종 환자의 임상 결과에 대한 유용한 영상 표지자로 검증되었다. 저혈관 세포 서식지의 증가는 초기 종양 진행과 진행 장소를 예측하는 강력한 영상 표지자로 기능할 수 있을 것으로 기대된다.